

## A segmented multi-loop antenna for selective excitation of azimuthal mode number in a helicon plasma source

S. Shinohara, T. Tanikawa, and T. Motomura

Citation: [Review of Scientific Instruments](#) **85**, 093509 (2014); doi: 10.1063/1.4896041

View online: <http://dx.doi.org/10.1063/1.4896041>

View Table of Contents: <http://scitation.aip.org/content/aip/journal/rsi/85/9?ver=pdfcov>

Published by the [AIP Publishing](#)

---

### Articles you may be interested in

[Investigations on loop antenna excited whistler waves in a cylindrical plasma based on laboratory experiments and simulations](#)

Phys. Plasmas **19**, 102113 (2012); 10.1063/1.4763558

[Resonant power absorption in helicon plasma sources](#)

Phys. Plasmas **13**, 123507 (2006); 10.1063/1.2402913

[Development of a strong field helicon plasma source](#)

Rev. Sci. Instrum. **77**, 036108 (2006); 10.1063/1.2173940

[Density profile control in a large diameter, helicon plasma](#)

Phys. Plasmas **12**, 057101 (2005); 10.1063/1.1863212

[Wave phenomena, hot electrons, and enhanced plasma production in a helicon discharge in a converging magnetic field](#)

Phys. Plasmas **11**, 3888 (2004); 10.1063/1.1764830

---

**Nor-Cal Products**



Manufacturers of High Vacuum  
Components Since 1962

- Chambers
- Motion Transfer
- Flanges & Fittings
- Viewports
- Foreline Traps
- Feedthroughs
- Valves



[www.n-c.com](http://www.n-c.com)  
800-824-4166

# A segmented multi-loop antenna for selective excitation of azimuthal mode number in a helicon plasma source

S. Shinohara,<sup>1,a)</sup> T. Tanikawa,<sup>2</sup> and T. Motomura<sup>3,b)</sup>

<sup>1</sup>*Institute of Engineering, Tokyo University of Agriculture and Technology, 2-24-16 Naka-cho, Koganei, Tokyo 184-8588, Japan*

<sup>2</sup>*Research Institute of Science and Technology, Tokai University, 4-1-1, Kita-kaname, Hiratsuka, Kanagawa 259-1292, Japan*

<sup>3</sup>*National Institute of Advanced Industrial Science and Technology (AIST), 807-1, Shuku-machi, Tosu, Saga 841-0052 Japan*

(Received 28 July 2014; accepted 6 September 2014; published online 29 September 2014)

A flat type, segmented multi-loop antenna was developed in the Tokai Helicon Device, built for producing high-density helicon plasma, with a diameter of 20 cm and an axial length of 100 cm. This antenna, composed of azimuthally splitting segments located on four different radial positions, i.e.,  $r = 2.8, 4.8, 6.8,$  and  $8.8$  cm, can excite the azimuthal mode number  $m$  of  $0, \pm 1,$  and  $\pm 2$  by a proper choice of antenna feeder parts just on the rear side of the antenna. Power dependencies of the electron density  $n_e$  were investigated with a radio frequency (rf) power less than 3 kW (excitation frequency ranged from 8 to 20 MHz) by the use of various types of antenna segments, and  $n_e$  up to  $\sim 5 \times 10^{12} \text{ cm}^{-3}$  was obtained after the density jump from inductively coupled plasma to helicon discharges. Radial density profiles of  $m = 0$  and  $\pm 1$  modes with low and high rf powers were measured. For the cases of these modes after the density jump, the excited mode structures derived from the magnetic probe measurements were consistent with those expected from theory on helicon waves excited in the plasma. © 2014 AIP Publishing LLC. [<http://dx.doi.org/10.1063/1.4896041>]

## I. INTRODUCTION

After recognizing the useful helicon discharges by pioneers' works, e.g., Refs. 1 and 2, high-density ( $\sim 10^{13} \text{ cm}^{-3}$ ) and low temperature (in the range of 1–10 eV) helicon sources<sup>3–8</sup> of various types based on the concept originally developed by Boswell,<sup>9</sup> have been extensively investigated. Now, many possible their applications can be seen in such as the fields of the industrial application of plasmas, nuclear fusion, and basic fields including space plasmas. For example, helicon sources are being utilized for the basic studies of Alfvén waves, magnetic reconnection, and plasma turbulences. In addition, a helicon source can be regarded as one of the important plasma sources for plasma thruster because of no electrodes directly contacting with plasma, leading to a longer lifetime operation. Needless to say, helicon sources can easily produce high-density plasmas with a broad range of external operating parameters, e.g., the fill pressure, the magnetic field strength, and its field configuration, as long as the excitation frequency is between the ion and electron cyclotron frequencies.

In the past, characterizations of various helicon sources by measuring profiles of electron density, light emission, and wave structures with a broad range of device size and external operation parameters have been extensively carried out. Concerning the excitation of the azimuthal mode number  $m$  in the helicon wave scheme,<sup>10</sup> many different types of antennas<sup>7,8</sup> have been tried. They are: (a) a single- or a multi-loop type antennas ( $m = 0$  excitation),<sup>11,12</sup> (b) an antenna with no helical

pitch (Boswell type)<sup>9</sup> and a double-saddle antenna (these two can excite  $m = \pm 1$  modes simultaneously because both modes are mixed), and (c) a (rotating) Nagoya type III antenna<sup>13,14</sup> and an antenna with a helical pitch (these two can excite  $m = 1$  or  $-1$  selectively by changing the direction of the magnetic field or an antenna current phase between different elements).<sup>15–17</sup> However, there have been few experiments in the  $m = \pm 2$  excitation up to now.<sup>18,19</sup> While the above antennas are wound around an insulation tube with a small radius, a spiral antenna for large diameter plasma ( $m = 0$  excitation) is located at the end of the chamber through an insulation window.<sup>20–22</sup>

As was mentioned before, antennas to excite  $m = 0$  and  $\pm 1$  (and  $m = 1$  if a single mode is excited) modes were used in the most of the past experiments, but there have been few experiments to compare directly the plasma performance, changing the mode number in the same device and the same antenna. Of course, also as was mentioned before, the comparative studies between  $m = 1$  and  $-1$  were tried by the use of an antenna with a helical pitch, because it was easy to carry out the experiments, by simply changing the direction of the magnetic field.<sup>16,23</sup> Although some data did not show any appreciable difference between the two modes, some data showed that  $m = 1$  mode was more or less preferentially excited compared to  $m = -1$  mode: while the wave with the  $m = 1$  mode could propagate axially with the higher electron density produced, the wave with  $m = -1$  mode showed the stronger axial damping, which was consistent with the numerical calculations.<sup>24</sup> There were few experiments to make a direct comparison between  $m = 0$  and  $1$  or  $-1$  modes using the same device but different antennas, and there was only one case<sup>19</sup> to compare the plasma behaviors between  $m = 1$  and 2

<sup>a)</sup>Electronic mail: sshinoha@cc.tuat.ac.jp.

<sup>b)</sup>This research was performed while T. Motomura was at IGES, Kyushu University, Kasuga, Fukuoka 816-8580, Japan.

modes with the same device but different antennas, as far as we know: the former mode has a peaked density profile, while the latter one has a broad profile, and these findings can be understood from the calculated power deposition profiles. Note that these studies of  $m = \pm 1$  and  $\pm 2$  modes were carried out with axially extended antennas and were not performed with a flat type antenna. Furthermore, the development of a spiral type antenna and the associated control of radial density profiles were so far carried out by our group only.<sup>21,22</sup>

Considering the conventional antenna system and their results mentioned above, we have designed a new category of an antenna, i.e., a segmented multi-loop antenna. In this paper, we will focus the following points: (1) Demonstration of the usefulness of an advanced spiral antenna installed at the end of a chamber for producing large diameter plasmas, compared to the smaller ones with the antenna wound around an insulator tube. (2) Direct comparison of plasma performance and wave structures between differential mode numbers of  $m = 0, \pm 1$ , and  $\pm 2$ , using the same device and the same antenna, which is crucial for the assessment of plasma performance and excited radio frequency (rf) wave structures. (3) Control of radiation field patterns, causing the change of the effective plasma radius produced, by selecting the antenna segments radially distributed. We have designed the segmented multi-loop antenna with the advantage of easily varying azimuthal mode excitations without taking time and efforts. What one needs to do is to simply change the connections of the antenna feeder points. In addition, the antenna and the impedance matching box are assembled side by side so as to reduce electrical noises and resistances in the electrical circuits. The whole assembly can be easily handled so that the changing antenna configuration is very easy, since this unit is movable along the axial direction.

Experiments on the selective excitation of waves with various  $m$  numbers and produced plasma performance have

been carried out, by using a developed medium-sized machine, the Tokai helicon device (THD). The outline of this paper is as follows. First, vacuum and magnetic field systems of the THD and the new type of segmented multi-loop antenna along with the rf system are described in Sec. II. Next, we will show the experimental results of the plasma performance (including photos of plasma light) such as the dependence of the electron density on the rf power, the radial density profiles with low- and high-density discharges, and the excited rf structures in the plasma, changing the  $m$  numbers, in Sec. IV. Finally, the concluding remarks of the experimental results using the newly developed antenna in the THD are presented in Sec. IV.

## II. DESCRIPTIONS OF THE THD DEVICE AND MULTI-LOOP ANTENNA

The THD is equipped with a specially designed, segmented multi-loop antenna to excite the helicon waves, as shown in Fig. 1. The vacuum chamber, in Figs. 1(a) and 1(c), made of stainless-steel has an inner diameter of 20 cm with an axial length of 100 cm. Here, the base pressure is kept at  $<10^{-4}$  Pa by using a diffusion pump (ULK-06A, ULVAC, Inc.: pumping speed of 1200 l/s) that is installed under the T-shaped chamber with the axial length of 60 cm [the right-hand side in Fig. 1(a)]. A diffusion pump is selected over a turbo-molecular pump so as not to worry about the high-frequency noise produced by a TMP. For the experiments presented in this paper, argon gas is fed through a needle valve with a fill pressure range of 0.3–1 Pa. In order to accept various diagnostics, the 16 side ports are provided in addition to the viewing ports at the end of the chamber.

Nine magnetic coils, 304 turns each with an indirect water cooling system, are installed around the vacuum chamber. They can produce a maximum field of 0.6 kG using the

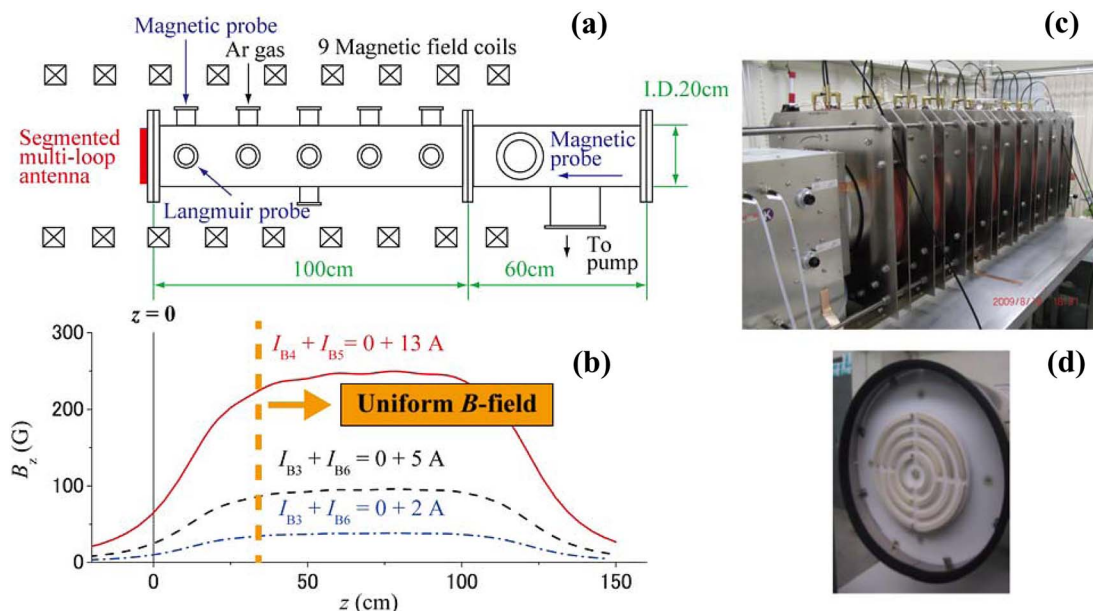


FIG. 1. A schematic diagram and photos of the Tokai Helicon Device (THD) and its segmented multi-loop antenna. Three examples of the calculated axial magnetic field profile at  $r = 0$  (central axis of the vacuum chamber) are also shown.

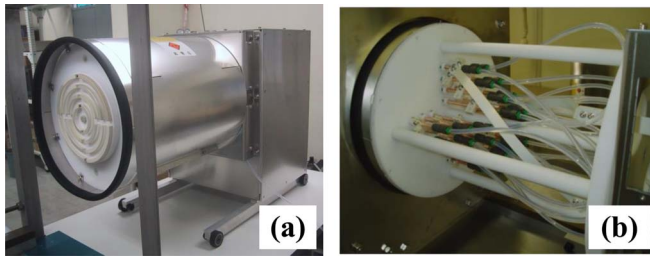


FIG. 2. Photos of (a) a segmented multi-loop antenna with a matching box and (b) electric feeder parts for an antenna connection and water cooling pipes on the rear side of the antenna.

presently available power supplies; however, the field strength can be increased up to a few kG level by adding an extra power supply. If all coils are connected in series, the uniformity of the magnetic field is within  $\pm 1.5\%$  in the whole region of the vacuum chamber. By a proper connection of the feeders of the magnetic coils and the use of two separate power supplies, the magnetic field configurations can be changed more flexibly. Figure 1(b) shows typical examples of the magnetic field profiles along the axial  $z$  direction. Note that the weaker field near the antenna makes it easier to obtain high-density helicon plasmas. This point will be described later. Here,  $I_{B4} + I_{B5} = 0 + 13$  A (a red, solid curve), where the currents in the first four coils from the far left are 0 A and those in the remaining five coils are 13 A. Likewise,  $I_{B3} + I_{B6} = 0 + 5$  A (a black, dotted curve) or  $0 + 2$  A (a blue, chain curve) means that the currents in the first three coils from the far left are 0 A and those in the remaining six coils are 5 A or 2 A, respectively.

The rf system consists of three parts: a flat type, segmented multi-loop antenna for plasma production, an impedance matching box, and an rf power supply. As was mentioned before, the former two have a unified structure, directly connected to each other, so as to reduce the rf noise and the loss due to the electrical resistance loss, as shown in Fig. 2(a). The whole antenna is covered by a stainless-steel shield and is installed just outside the quartz-glass window with 15 mm thickness at the left end of the vacuum chamber in Fig. 1(a). The antenna, located at an axial distance of 10 mm from the quartz-glass surface, consisted of four concentric copper loops with a square shape cross-section of 0.85 cm long, which are hollow to allow cooling water to flow.

Each of three outer loops is divided into four equal segments, and the central loop is two equal segments. Here, the radial positions of these four loops are 2.8, 4.8, 6.8, and 8.8 cm, respectively. By varying the electrical connections between the antenna segments, it is possible to excite, not only the waves with  $m = 0$  but also those with  $m = \pm 1$  and  $\pm 2$  as well, as shown in Fig. 3. In this figure, snapshots of the rf antenna current directions are shown. Here, the innermost to outermost loops are dubbed I–IV. Using the four radial locations of the antenna segments, radiation field patterns (radial profiles) can be changed: e.g., the use of #I (all use of #I, #II, #III, and #VI) makes a smaller (larger) size of radiation pattern and an outer loop only makes a hollow radiation pattern. In Fig. 2(b), this electrical connection on the rear side of antenna loops along with water cooling pipes can be seen.

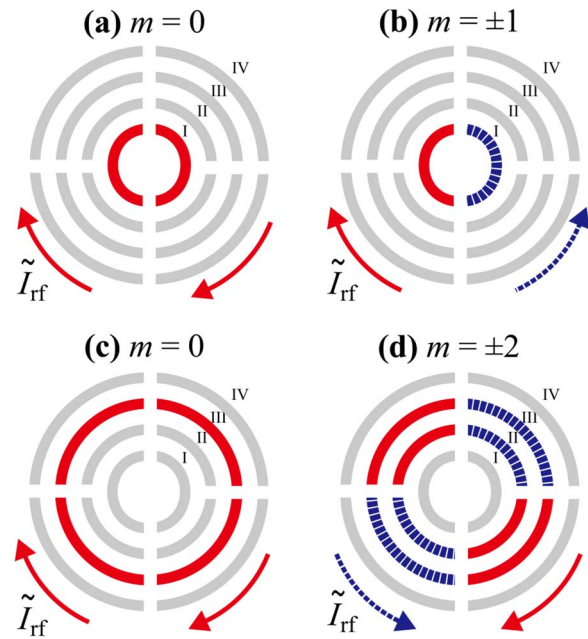


FIG. 3. A schematic of rf antenna current with connections between multi-loop segments viewed from the axial direction. Here, the innermost segments to the outermost loops are dubbed I–IV. Alternating rf current directions, in red and dark blue, presented here shows a snapshot. Here, examples are shown for the excitations of  $m =$  (a) 0 (the use of #I loop segments), (b)  $\pm 1$  (#I), (c) 0 (#III), and (d)  $\pm 2$  (#II and #III in a series connection).

The matching box, right-hand side in Fig. 2(a) has a split tank circuit: variable vacuum and fixed capacitors are used in the parallel (4500 pF in total) and series (4000 pF in total) electrical connections. Since this box can be easily moved with four small casters, as shown in Fig. 2(a), the setting up and dismantling of the entire antenna assembly with the matching circuit near the quartz window at the end of the vacuum chamber are simple tasks [see the left-hand side in Fig. 1(a)]. In order to estimate an rf antenna-plasma coupling, the rf current and voltage of the antenna are measured in addition to measuring the incident and reflected powers (these monitors are attached in this box). The rf power supply (T146-6656A, THAMWAY) can feed its power up to 2 (4) kW in a continuous (pulsed) operation mode, with an rf frequency  $f$  of 5–40 MHz and a pulse modulator (T090-1046A, THAMWAY). Due to heat damages to Langmuir and magnetic probes, our experiments were carried out in a 50 ms rf discharge pulse with a 1 s interval (duty ratio was 1/20).

Next, we will describe the measuring system. As was mentioned before, the 16 side ports of the vacuum chamber, located on between the neighboring magnetic coils, can be used for diagnostic instruments along with the side and the end ports in the T-shaped chamber. A Langmuir probe for electron density and temperature measurements had a disk type electrode, 0.5 cm in diameter, and was located at the axial position of  $z = 30$  cm, where  $z = 0$  is defined as the left flange surface of the vacuum chamber [see Fig. 1(a)]. Three magnetic probes with a one-turn loop (1 cm in diameter) each, using a semi-rigid cable, can measure the  $B_\theta$  or  $B_z$  components of the excited rf magnetic field (wave measurements) in the plasma. Here, this rotatable, loop antenna can be scanned

radially (at  $z = 30$  cm) or axially (from the end of the chamber). A standard digital camera and a high-speed one for optical measurements were used through a glass window on the side or end ports of the chamber.

### III. EXPERIMENTAL RESULTS

First, typical examples of plasma light are shown in Fig. 4. They are taken by a standard digital camera from the end of the vacuum vessel with the net rf power of  $P_{\text{net}} \sim 2$  kW. Here,  $P_{\text{net}}$  is defined as  $P_{\text{inpi}} \times R_p / (R_v + R_p)$ , where  $R_v$  and  $R_p$  are the vacuum and plasma loading resistances, respectively, and  $P_{\text{inpi}}$  is the difference between the incident and reflected rf powers. Figure 4(a) is the case of  $m = 0$  with the use of #I antenna loop segments,  $I_{B3} + I_{B6} = 0 + 5$  A, and  $f = 20$  MHz. Similarly, Fig. 4(b) [4(c)] is the case of  $m = \pm 1$  ( $\pm 2$ ) excitation mode with #I (#II and #III in a series connection) loop segments,  $I_{B4} + I_{B5} = 0 + 13$  A ( $I_{B3} + I_{B6} = 0 + 5$  A), and  $f = 8$  (15) MHz. The former two cases had the stronger argon blue light, showing a higher electron density  $n_e$ , compared to

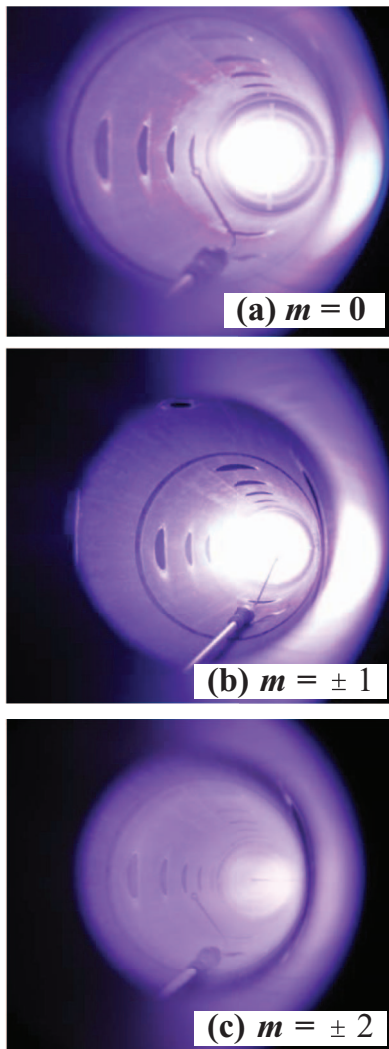


FIG. 4. Typical plasma light taken from the end of the chamber [right hand side in Fig. 1(a)], viewing the antenna and an inner wall of the vacuum chamber for the cases of  $m =$  (a) 0, (b)  $\pm 1$ , and (c)  $\pm 2$  excitations. Side port holes and a magnetic probe can be also seen.

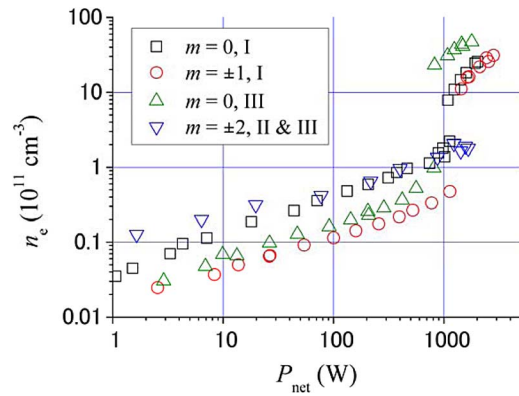


FIG. 5. Electron density  $n_e$  as a function of rf net power  $P_{\text{net}}$  for different excitations of azimuthal mode numbers. Here, radial positions of antenna loop segments used with mode number  $m$  are also shown.

the last one. Axial plasma light intensity profiles using the five side viewing ports also showed the similar tendency: plasma light intensity was weaker in the last case compared to the former two cases and the intensity in each case decreased away from the antenna. Here in this section, unless specified, the magnetic field distribution and the rf frequency in each mode were the same as described above with an argon fill pressure kept constant at 0.38 Pa.

Next, we will present plasma performance, using our newly developed antenna. Figure 5 shows dependencies of  $n_e$ , measured at  $z = 30$  cm and at the plasma center of  $x$  (radial position) = 0, as a function of  $P_{\text{net}}$ , in the various azimuthal modes:  $m = 0$  (note that  $f$  was 8 MHz by the use of #III loop segments),  $\pm 1$ , and  $\pm 2$ . Here, typical efficiency  $\eta = R_p / (R_v + R_p)$ , showing a power coupling to the plasma, was  $>60\%$  in the high-density discharges. From this figure, a low-density plasma ( $n_e < 10^{10}$  cm $^{-3}$ ), regarded as Capacitively Coupled Plasma (CCP), could be initiated with  $P_{\text{net}}$  as low as  $\sim 1$  W range, which is typical and advantageous for the cases of spiral antennas<sup>21,22</sup> located at the end of the vacuum chamber. With increasing  $P_{\text{net}}$  from  $\sim 1$  to  $\sim 1000$  W,  $n_e$  increased almost continuously from  $10^9$  to  $10^{11}$  cm $^{-3}$  ranges in all different  $m$  modes.

After exceeding threshold powers  $P_{\text{th}} \sim 1000$  W,  $n_e$  increased drastically by one order of magnitude to  $>10^{12}$  cm $^{-3}$ , which is so-called “a density jump”<sup>25</sup> in all modes except for  $m = \pm 2$  mode. This jump, accompanied by a jump of the light intensity from the weaker to the stronger blue light as well as a  $R_p$  jump, could be regarded as a mode change from Inductively Coupled Plasma (ICP) to Helicon Plasma (HP), whose rf wave structures will be discussed later. There was a tendency that  $P_{\text{th}}$  was slightly higher in the case of  $m = \pm 1$  than that of  $m = 0$ . Before the density jump ( $P_{\text{net}} < 1$  kW range), a sequence from higher to lower densities with the same rf power range was as follows:  $m = \pm 2$  mode (#II and #III loop segments),  $m = 0$  (#I),  $m = 0$  (#III), and  $m = \pm 1$  (#I). On the other hand, after the density jump, this sequence was changed as follows:  $m = 0$  mode (#III segments),  $m = 0$  (#I), and  $m = \pm 1$  mode (#I), where  $m = \pm 2$  mode (#II and #III loop segments) showed the lowest density because of no density jump, as was mentioned before. These density differences in the low and high rf power cases will be discussed later

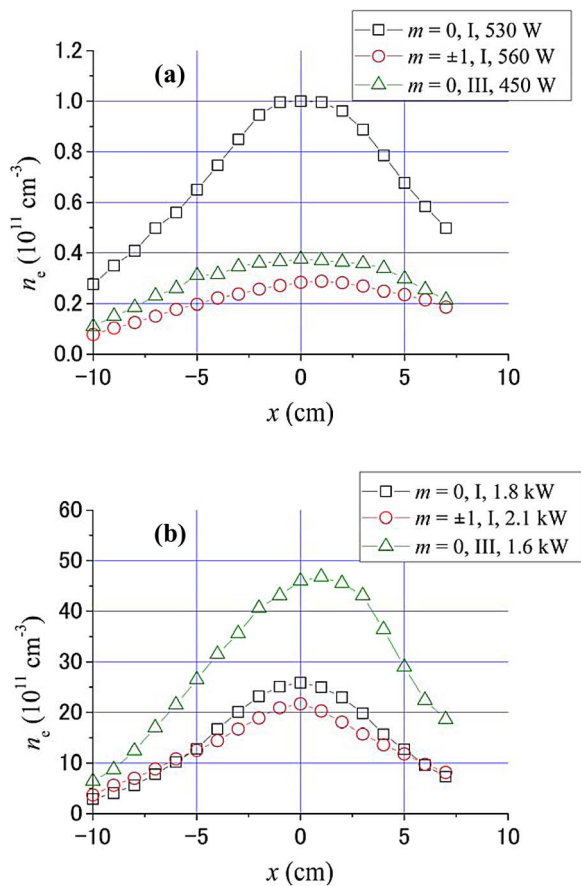


FIG. 6. Radial profiles of electron density  $n_e$  with (a) low and (b) high rf net powers for different excitations of azimuthal mode numbers. Here, mode number  $m$ , radial positions of antenna loop segments used, and rf net power  $P_{\text{net}}$  are also shown.

in Fig. 6. Concerning the  $P_{\text{th}}$  value, other experiments with  $m = 0$  excitation (not shown) showed that the weaker magnetic field near the antenna, in other words, the convergent magnetic field, was better to have a smaller  $P_{\text{th}}$  value (and  $n_e$  was smaller after the jump). This is consistent with the previous results, using a spiral antenna,<sup>26</sup> as well as the experimental<sup>27</sup> and numerical<sup>28</sup> results for the case of loop antennas wound around the insulation tube.

Although high-density helicon modes were found in other experiments<sup>18,19</sup> with the use of  $m = \pm 2$  or 2 modes antennas wrapped around the quartz tubes, the reason why we could not find a density jump in the  $m = \pm 2$  mode experiments, including the following connection cases of loop segments of #II, or #IV, or #II + #IV (series connection), was not clear. Considering that the expected deposition profile is broader with  $m = 2$  mode compared to  $m = 1$  mode,<sup>19</sup> which may change the radial particle transport, higher rf power trials may be necessary to check the existence of HP mode, varying external parameters. Note that, compared to ours, their antennas<sup>18,19</sup> were wound around the smaller tube diameters, 10 and 14.6 cm with the higher magnetic fields of several hundred G. In addition to an rf power discussion, in our case, the stronger rf coupling (interference) between neighboring antenna elements than that for the  $m = 0$  and  $\pm 1$  excitation was found, due to a smaller size of each segment current for this

$m = \pm 2$  excitation. This leads to a difficulty of an impedance matching, and hinders the efficient delivered power to an antenna with  $m = \pm 2$  excitation mode. Along with a special care of this matching with a higher rf power, we may need longer segments, using larger antenna radius in a larger chamber to have a longer distance in the radial and azimuthal directions between neighboring segments.

Radial profiles of  $n_e$  were investigated with the low-density (with low rf power) and high-density (with high rf power) modes, as shown in Fig. 6, changing the mode number and antenna loop segments in the radial location. Low-density ( $< 10^{11} \text{ cm}^{-3}$ ) case in Fig. 6(a) showed that  $n_e$  with  $m = 0$  was higher than that with  $\pm 1$  mode with the use of the same loop segments of #I, in spite of the weaker magnetic field for the  $m = 0$  case. With the same mode of  $m = 0$ ,  $n_e$  was higher using #I loop segments, located in the inner region, than #III loop segments, which may be due to the better confinement in the inner region, where each segments is expected to produce plasma just near its region in the ICP mode due to the near field effect. In addition, this reason may be partly because that the rf frequency used was different: the former (latter) was 20 (8) MHz. In fact, #III loop segments showed the broader profile than #I loop segments due to the ICP discharge again, where #III loop segments were located in the outer radial region compared to #I segments.

Similarly, high-density ( $> 10^{12} \text{ cm}^{-3}$ ) case in Fig. 6(b) showed that  $n_e$  was higher with  $m = 0$  than  $\pm 1$  modes with the use of the same loop segments of #I. Considering that the peaked power deposition from a collisional damping is expected to be the central part because of  $J_0^2$  form (off-axis part because of  $J_1^2$  form) for the helicon  $m = 0$  ( $\pm 1$ ) mode<sup>10</sup> (although in some experimental cases,  $m = \pm 1$  mode had not a broad profile<sup>10</sup>), this can be partly interpreted as the better confinement efficiency in the central region than the intermediate radial region. Here,  $J_0$  and  $J_1$  are Bessel functions of the first kind. For the case of the high-density discharges, a rough estimate of particle production efficiency, i.e., total number of particles in the whole volume divided by rf power, was executed and this shows a very excellent efficiency: only by a factor of a few times lower than the predicted value<sup>29</sup> (see also Fig. 4 in Ref. 30 concerning this production scaling law) based on the elementary process and classical diffusion. Here, this predicted, ideal confinement time is considered to be an upper limit. On the other hand, with the same mode of  $m = 0$ ,  $n_e$  was higher using #III loop segments than #I loop segments, which was different in the low-density (low rf power) mode and whose reason is not clear. The radial  $n_e$  profile for the case of #III loop segments showed a somewhat broader profile than that for the case of #I loop segments (this difference was smaller than that for the low-density, low rf power case). This is partly due to the helicon mode excitation in the high-density discharge, i.e., fixed wave structures in the radial direction constrained by the boundary makes the nearly same power deposition profile, regardless of the antenna radiation pattern once helicon wave is excited. The radial  $n_e$  profiles with low-density mode were consistent with the previous results<sup>26</sup> using a spiral antenna that it is important to produce the plasma near the antenna region.

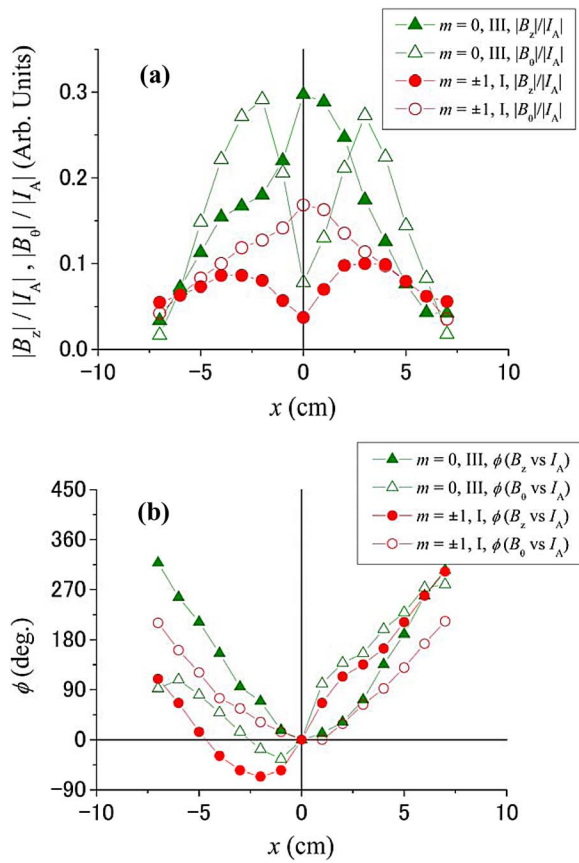


FIG. 7. Radial profiles of (a) the axial  $|B_z|$  or azimuthal  $|B_\theta|$  components of the rf excited magnetic fields normalized by the antenna rf current  $|I_A|$  and (b) the phase  $\phi$  between the field components,  $B_z$  or  $B_\theta$ , and  $I_A$  for the excitations of azimuthal mode numbers of  $m = 0$  and  $\pm 1$ . Here, mode number, radial positions of antenna loop segments used, and the field components are also shown.

Finally, we have investigated the rf wave structures of  $m = 0$  (the use of #III loop segments) and  $\pm 1$  (the use of #I loop segments) modes in Fig. 7, under the same experimental conditions of Fig. 6. Here,  $m = \pm 2$  case was not included due to the lower density, i.e., no density jump showing non-helicon behavior, compared to the  $m = 0$  and  $\pm 1$  modes, and the lower light intensity with  $P_{\text{net}}$  of 1–2 kW, as was previously mentioned (see Figs. 4 and 5). For the case of  $m = 0$  excitation, axial (azimuthal) component of rf magnetic field  $B_z$  ( $B_\theta$ ) is expected to have a radial profile of Bessel function  $J_0$  ( $J_1$ ) shape in the helicon wave excitation under the flat radial density profile.<sup>10</sup> Similarly, for the case of  $m = \pm 1$  excitation,  $B_z$  ( $B_\theta$ ) is expected to have a radial profile of  $J_1$  (linear combination of  $J_0$  and  $J_1$ ) under the flat radial density profile.<sup>10</sup>

Radial profiles of amplitudes of  $B_z$  and  $B_\theta$  normalized by the amplitude of the antenna current  $I_A$  for  $m = 0$  and  $\pm 1$  modes in Fig. 7(a) agreed well with these theoretical expectations of helicon waves, mentioned above. From the theory,<sup>10</sup> for the case of  $m = 0$  excitation,  $B_z$  ( $B_\theta$ ) is expected to change a sign at the plasma periphery (center), and for the case of  $m = \pm 1$  excitation,  $B_z$  is expected to change a sign at the plasma center. These were also consistent with the experimental results in Fig. 7(b), showing the radial profiles of the phase between the  $B_z$  (or  $B_\theta$ ) and antenna current. From the

rough measurements of the wave excited  $B_z$  profiles along the  $z$  axis to derive a parallel wavelength also supported the helicon wave dispersion relation (not shown).

#### IV. CONCLUSION

In summary, in order to execute an advanced high-density helicon study, a selected excitation of the azimuthal mode, i.e.,  $m = 0, \pm 1$ , and  $\pm 2$ , using a developed, segmented multi-loop antenna was demonstrated in the THD, with a diameter of 20 cm and an axial length of 100 cm. Our new type of antenna has azimuthally splitting segments located at four different radial positions. We have investigated plasma performance and excited rf wave structures, changing the mode number and the radial radiation field distribution. The dependencies of  $n_e$  on  $P_{\text{net}}$  were measured under different azimuthal modes with  $P_{\text{net}}$  less than 3 kW, and  $n_e$  up to  $\sim 5 \times 10^{12} \text{ cm}^{-3}$  was obtained after the density jump with  $f = 8\text{--}20 \text{ MHz}$ . Radial profiles of  $n_e$  were also measured and discussed under the different conditions. From the rf wave measurements, it was demonstrated that  $m = 0$  and  $\pm 1$  helicon modes, expected from theories, were excited after the density jump. Although useful data on helicon high-density discharges using this new antenna were obtained successfully, further studies are necessary such as the checking of the existence of a density jump to enter a helicon discharge for  $m = \pm 2$  mode, and various connection experiments using radially, azimuthally distributed loop segments, changing external parameters.

These results are very useful for many future fundamental and application studies. For example, this device of THD was originally developed to produce a high-density HP by this specially designed antenna that could be used for a variety of nonlinear wave experiments to simulate the space plasma phenomena.

#### ACKNOWLEDGMENTS

This work has been partially supported by Grant-in-Aid for Scientific Research (S: 21226019) from the Japan Society for the Promotion of Science. This paper is dedicated to the memory of late Dr. K. P. Shamrai.

- <sup>1</sup>J. P. Klosenber, B. McNamara, and P. C. Thonemann, *J. Fluid Mech.* **21**, 545 (1965).
- <sup>2</sup>J. A. Lehne and P. C. Thonemann, *Proc. Phys. Soc.* **85**, 301 (1965).
- <sup>3</sup>M. A. Lieberman and A. J. Lichtenberg, *Principles of Plasma Discharges and Materials Processing* (Wiley, New York, 1994), p. 434.
- <sup>4</sup>S. Shinohara, *Jpn. J. Appl. Phys., Part 1* **36**, 4695 (1997) (Review Paper) and references therein.
- <sup>5</sup>R. W. Boswell and F. F. Chen, *IEEE Trans. Plasma Sci.* **25**, 1229 (1997) (Review Paper) and references therein.
- <sup>6</sup>F. F. Chen and R. W. Boswell, *IEEE Trans. Plasma Sci.* **25**, 1245 (1997) (Review Paper) and references therein.
- <sup>7</sup>S. Shinohara, *J. Plasma Fusion Res.* **78**, 5 (2002) (Review Paper) and references therein (in Japanese).
- <sup>8</sup>S. Shinohara, *Butsuri* **64**, 519 (2009) (Review Paper) and references therein (in Japanese).
- <sup>9</sup>R. W. Boswell, *Phys. Lett.* **33A**, 457 (1970).
- <sup>10</sup>F. F. Chen, *Plasma Phys. Controlled Fusion* **3**, 339 (1991).
- <sup>11</sup>Y. Sakawa, N. Kinoshita, and T. Shoji, *Appl. Phys. Lett.* **69**, 1695 (1996).
- <sup>12</sup>S. Shinohara, N. Kaneda, and Y. Kawai, *Thin Solid Films* **316**, 139 (1998).
- <sup>13</sup>T. Watari, *Phys. Fluids* **21**, 2076 (1978).

- <sup>14</sup>Y. Yasaka and Y. Hara, *Jpn. J. Appl. Phys.* **33**, 5950 (1994).
- <sup>15</sup>M. Light and F. F. Chen, *Phys. Plasmas* **2**, 1084 (1995).
- <sup>16</sup>S. Shinohara, Y. Miyauchi, and Y. Kawai, *Plasma Phys. Controlled Fusion* **37**, 1015 (1995).
- <sup>17</sup>A. Degeling, C. O. Jung, R. W. Boswell, and A. R. Ellingboe, *Phys. Plasmas* **3**, 2788 (1996).
- <sup>18</sup>J.-H. Kim, S.-M. Yun, and H.-Y. Chang, *IEEE Trans. Plasma Sci.* **24**, 1364 (1996).
- <sup>19</sup>M. Krämer, B. Lorenz, and B. Clarenbach, *Plasma Sources Sci. Technol.* **11**, A120 (2002).
- <sup>20</sup>J. E. Stevens, M. J. Sowa, and J. L. Cecchi, *J. Vac. Sci. Technol. A* **13**, 2476 (1995).
- <sup>21</sup>S. Shinohara, S. Takechi, and Y. Kawai, *Jpn. J. Appl. Phys.* **35**, 4503 (1996).
- <sup>22</sup>S. Shinohara and T. Tanikawa, *Rev. Sci. Instrum.* **75**, 1941 (2004).
- <sup>23</sup>F. F. Chen, I. D. Sudit, and M. Light, *Plasma Sources Sci. Technol.* **5**, 173 (1996).
- <sup>24</sup>I. V. Kamenski and G. G. Borg, *Phys. Plasmas* **3**, 4396 (1996).
- <sup>25</sup>A. R. Ellingboe and R. W. Boswell, *Phys. Plasmas* **3**, 2797 (1996).
- <sup>26</sup>S. Shinohara and T. Tanikawa, *Phys. Plasmas* **12**, 044502 (2005).
- <sup>27</sup>S. Shinohara and K. Yonekura, *Plasma Phys. Controlled Fusion* **42**, 41 (2000).
- <sup>28</sup>S. Shinohara and K. P. Shamrai, *Plasma Phys. Controlled Fusion* **42**, 865 (2000).
- <sup>29</sup>T. Tanikawa and S. Shinohara, in *Proceedings of 12th International Congress on Plasma Physics, Nice, France, 25–29 October 2004* (Association EURATOM-CAE, Cadarache, 2004), pp. 1–42, see <http://hal.archivesouvertes.fr/hal-00002013/en/>.
- <sup>30</sup>S. Shinohara, T. Hada, T. Motomura, K. Tanaka, T. Tanikawa, K. Toki, Y. Tanaka, I. Funaki, and K. P. Shamrai, *Phys. Plasmas* **16**, 057104 (2009).